UC San Diego

UC San Diego Previously Published Works

Title

Effects of electrode pattern on thermal runaway of lithium-ion battery

Permalink

https://escholarship.org/uc/item/87n492gg

Journal

International Journal of Damage Mechanics, 27(1)

ISSN

1056-7895

Authors

Wang, Meng
Le, Anh V
Noelle, Daniel J
et al.

Publication Date

2018

DOI

10.1177/1056789516660176

Peer reviewed

eScholarship.org Powered by the California Digital Library
University of California

Check for updates

Article

INTERNATIONAL JOURNAL OF DAMAGE MECHANICS

International Journal of Damage Mechanics
2018, Vol. 27(1) 74–81
© The Author(s) 2016
Reprints and permissions:
sagepub.co.uk/journalsPermissions.nav
DOI: 10.1177/1056789516660176
journals.sagepub.com/home/ijd
SAGE

Effects of electrode pattern on thermal runaway of lithium-ion battery

Meng Wang[1], Anh V Le[1], Daniel J Noelle[2], Yang Shi[2], Hyojung Yoon[3], Minghao Zhang[3], Y Shirley Meng[3] and Yu Qiao[1,2]

Abstract

In the current study, through a set of nail penetration and impact tests on modified lithium-ion battery coin half-cells, we examine the effects of electrode pattern on the heat generation behaviors associated with internal shorting. The results show that the temperature profile is quite insensitive to the openings in cathode layer, which may be attributed to the high specific energy as well as the secondary conductive paths. This finding will considerably influence the study in the area of thermal runaway mitigation of energy storage systems.

Keywords

Thermal runaway, lithium-ion battery, electrode pattern, impact, nail penetration

Introduction

Lithium (Li)-ion battery has a high energy density and a broad power range, attractive to a wide variety of applications (Liu et al., 2010). At the cell level, the specific energy of a commercially available Li-ion battery can be 200–250 W h/kg, and the records in research labs are two times higher (e.g. Iwamura et al., 2015). At the module or pack level, the specific energy is usually lower by ~50%. A major concern that often limits the application of Li-ion batteries is their safety, particularly thermal runaway (Bandhauer et al., 2011). Because Li is inherently reactive, the electrolyte must be based on organic solvents, such as dimethyl carbonate (DME) and ethyl methyl carbonate (EMC). Such electrolytes are highly flammable. Their combustion heats are around 14.5–21.5 kJ/g, approximately one half of that of gasoline (Harris et al., 2009). More critically, a charged

[1]Department of Structural Engineering, University of California—San Diego, La Jolla, USA
[2]Program of Materials Science and Engineering, University of California—San Diego, La Jolla, USA
[3]Department of Nanoengineering, University of California—San Diego, La Jolla, USA

Corresponding author:
Yu Qiao, Department of Structural Engineering, University of California—San Diego, La Jolla, CA 92093-0085, USA.
Email: yqiao@ucsd.edu

Li-ion battery has a high energy density. If the stored energy is rapidly dissipated, local temperature can drastically increase. When temperature rises to above 100–110°C, the decomposition of electrolyte and the electrochemical reactions speed up and become increasingly exothermal. Eventually, the battery may catch on fire.

Thermal runaway can be triggered by mechanical or thermal abuse. In a regular Li-ion battery, cathodes, membrane separator, and anodes form an alternately layered structure (Etacheri et al., 2011). As the battery cell is working normally, the membrane separator, usually made of a porous polystyrene, polypropylene (PP), and/or polyethylene (PE) sheet with the pore size around 20–100 nm and the thickness around 20–30 μm, keeps the anode and the cathode away in close proximity. Thus, internal shorting would not happen while the internal impedance is minimized. The porosity of the membrane separator is usually ~40%, and the mechanical properties can be highly anisotropic (Zhang, 2007). Along different directions, the membrane strength varies in the range from a few to dozens of MPa. Due to the small thickness and the relatively low strength, as the battery is subjected to a large external loading, such as an impact force, the membrane separator can rupture, causing internal shorting between the cathode and the anode in the damaged areas. Consequently, a large internal current is generated, accompanied by a rapid heat release. While this is often not an issue for small coin cells, for a large energy storage system, the temperature in the interior can quickly rise to more than ~110°C, beyond the safety range. It has been a major challenge to the Li-ion batteries that must remain safe under adverse conditions (Lu et al., 2007).

Over the years, many thermal-runaway mitigation approaches were studied. An attractive concept is to increase the internal impedance of the battery system when the membrane separator is damaged. For instance, Feng et al. (2004) used positive thermal coefficient (PCT) additives in the electrodes. As temperature rises to a set point, the PCT additives become electrically nonconductive, and thus, reduce the internal shorting current. Similar results may be achieved by using a low-melting-point (LMT) membrane separator (Balakrishnan et al., 2006): As the membrane melts and closes its pores, the ion conductivity may be decreased.

Recently, we investigated damage homogenizers (DH). A DH can be fine carbon particulates, such as carbon black (CB) microparticles (Le et al., 2015a) or bundles of carbon nanotubes (Le et al., 2015b). They are embedded in cathode and/or anode, with the particle size being a fraction of the electrode thickness. When the battery is impacted, the DH particles store and release sufficient elastic energy, which promotes the widespread disintegration of electrodes. Much faster than the PCT additives and the LMT membranes, the DH additives can increase the internal impedance immediately as the external mechanical loading is applied, before the heat generation begins. However, inconsistent experimental results were observed in various DH-modified battery cells: As a cell is damaged and internal shorting occurs, the postpeak temperature decrease rate can be largely reduced, yet the initial temperature increase rate and the peak temperature may not be affected. In the current study, we investigate an "extreme" case of electrode design with large openings, so as to evaluate the upper limit of the DH effects.

Experimental

The positive electrode contained 93 wt% $LiNi_{0.5}Mn_{0.3}Co_{0.2}O_2$ (NMC532) obtained from Toda America (Product No. NCM-04ST), 4 wt% polyvinylidene fluoride (PVDF) obtained from Sigma Aldrich (Product No. 182702), and 3 wt% Timcal CNERGY-C65 CB. The average particle size of NMC532 was around 15 μm; the average molecular weight of PVDF was 534 k. About 5 g of the mixture of NMC532, PVDF, and CB powders were ground for about 45 min in an agate mortar by a pestle and dissolved in 2 ml n-methyl-2-pyrrolidone in a 10 ml beaker. The solution was vigorously

stirred by a Qsonica Q55 probe for 10 times, with the mixing time and time interval of ~1 min. Then, 200 μm thick slurry was casted on an 18 μm thick aluminum sheet, by using a doctor blade. The wet slurry was vacuum dried in a VWR vacuum oven for 24 h at 100°C, and its thickness shrank to about 100–110 μm. The dried slurry was cold-rolled by a hardened steel double roller to the final thickness of 70–80 μm, and cut into disks, with the diameter of 14.3 mm. A ring opening was created in the condensed slurry disk by a razor blade, with the inner diameter of 6.35 mm and the outer diameter of 7.94 mm. Two 1.6 mm wide strips were left in the electrode film, bridging the inner and the outer parts together. Reference disk electrodes were produced through a similar method, except that the slurry was continuous and the outer diameter of the disk was 12.7 mm. The mass of NMC532 in a reference electrode was 20–22 mg. The mass of NMC532 in an electrode with ring opening was slightly lower than the theoretical value, around 21 ± 1 mg, due to the materials loss in the cutting procedure.

The electrode disks were assembled into CR2016 coin cells. In each cell, the cathode was directly placed on the stainless steel cell case; the cell case served as a charge collector. The cell cases were obtained from Xiamen Tob New Energy Technology Co., Ltd, with the product number of T-2016. Other components of the cell included a 25 μm thick microporous PP/PE/PP trilayer membrane separator (Product No. 2325, Celgard), a 15.6 mm diameter and 1.1 mm thick Li disk anode, forming a layer stack. About 30 ml BASF SelectiLyte-LP50 EMC solution was added. The cells were set at room temperature for more than 24 h.

Each cell was fully charged and discharged for 10 cycles between 3 and 4.3 V by an eight-channel battery analyzer (Item No. BST8-3, MTI Corp.), to verify its initial electrochemical performance and the discharge capacity. Then, the cell was charged to 4.6 V and was at rest for 2 h. For nail penetration testing, an Omega TT-K-40-25 type-K gage 40 thermocouple was attached to the upper surface of the cell by a duct tape, about 2 mm away from the center. The thermocouple was connected to an Omega OM-EL-USB-TC temperature logger. The cell was placed on a solid polyurethane (PU) stage in a Palmgren bench vise, and a 1/16″ diameter steel nail was driven through its center point (Figure 1). The coin cell and the nail were sealed by a layer of 1 cm thick PU foam. The temperature change was measured by the thermocouple, as shown in Figure 2. Altogether five CR2016 reference cathode half cells and five modified cathode half cells were tested.

We also investigated the behaviors of the reference and the modified cells in impact tests. The battery cell was firmly attached on a solid PU stage by insulating tapes, on top of which a brass spherical indenter was placed; the diameter of the indenter was 12.7 mm. An Omega TT-K-40-25

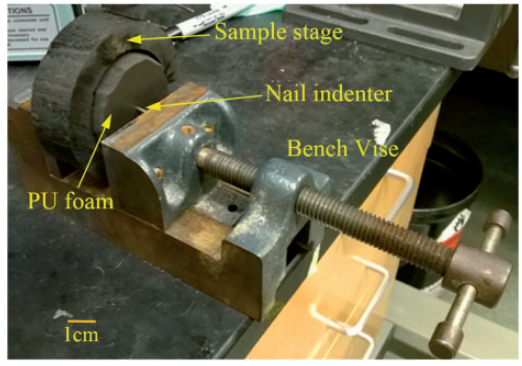

Figure 1. The nail penetration experimental setup. The battery cell is embedded in the PU foam and is not shown.

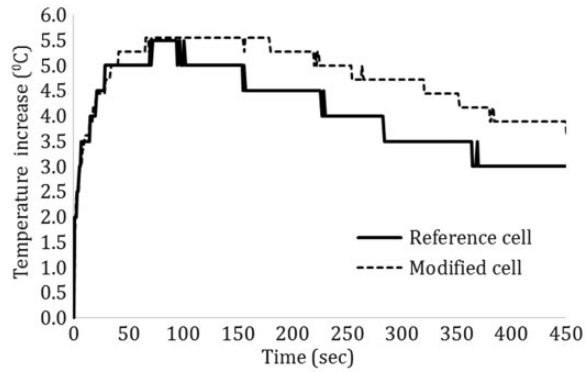

Figure 2. Typical temperature profiles in nail penetration tests.

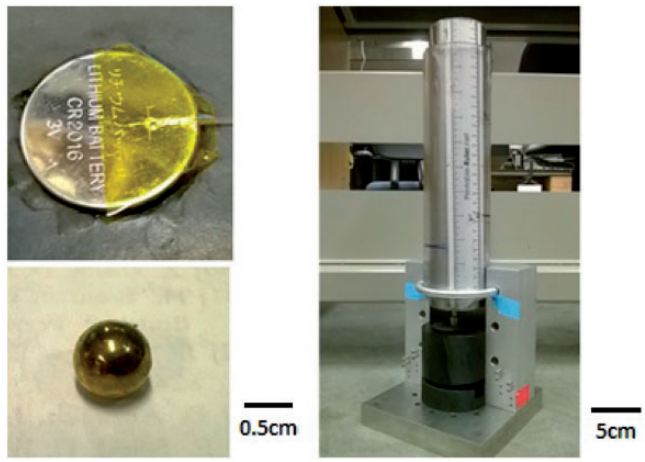

Figure 3. Photos of the impact experimental setup. Upper left: a CR2016 battery cell with a thermocouple attached on its upper surface; lower left: a copper spherical indenter; right: the table-top drop tower.

type-K gage 40 thermocouple was attached to the upper surface of the cell by insulating tapes, 3.7 mm away from the center. The thermocouple was connected to the Omega OM-EL-USB-TC temperature logger. To minimize the heat conduction, the indenter and the cell sample were separated by five layers of insulating tapes, and they were sealed by a solid PU cover, which also provided the guiding track to the incident rod (Figure 3). The incident rod was made of stainless steel; its diameter was 12.7 mm and its length was 50.8 mm. Initially, the rod was at rest on the indenter. A stainless steel cylindrical hammer was dropped on the incident rod from a distance of 16 cm. The diameter of the hammer was 62 cm; its height was 305 cm; the hammer mass was 7.7 kg. The hammer was guided by a vertical polycarbonate tube. Upon impact, the temperature variation of the battery was recorded by the thermocouple, as shown in Figure 4. Altogether five reference cathode half cells and five modified cathode half cells were tested. It was noticed that even impacting a fully discharged cell would cause a temperature increase of about 2.5°C, probably because of the plastic deformation and rupture of the cell case as well as the friction among the cell components.

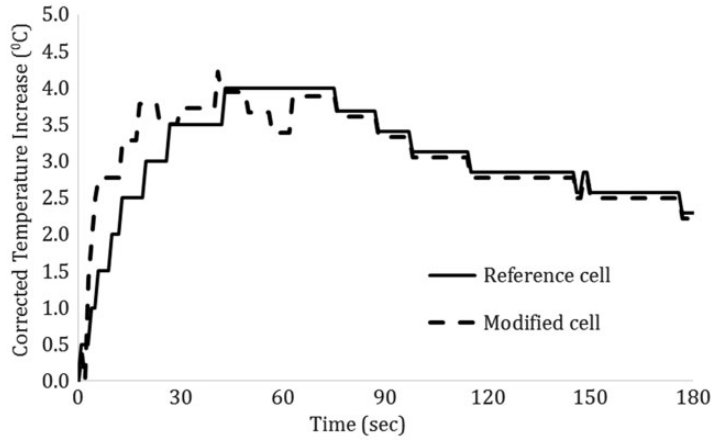

Figure 4. Typical temperature profiles in impact tests.

The average temperature profile of system bias, which was not associated with the stored electric energy in the electrode, was subtracted from the curves in Figure 4.

After the nail penetration and the impact tests, the cells were disassembled. The electrode layers were detached from the charge collectors. Typical photos of tested reference and modified electrodes are shown in Figure 5.

Results and discussion

In a nail penetration test, the metallic nail breaks the membrane separator and provides an electrically conductive shorting path between the cathode and the anode. Thus, a large internal current is generated. The forward path is from the cathode to the anode through the nail; the return path is from the anode to the cathode through the surrounding electrode area. The electrode potentials of the cathode and the anode are relatively stable. The heat generation rate associated with the internal shorting can be assessed as $U = V^2/R$, where V is the voltage between cathode and anode and $R = \rho t/A$ is the volume resistance, with ρ being the overall resistivity, t the electrode thickness, and A the involved area of electrode. In a battery cell, the resistivities of the cathode layer, the electrolyte, and the anode are low. Therefore, the heat generation rate is quite high, causing a rapid temperature increase, ΔT. In less than 1 min, the peak ΔT is achieved, followed by a plateau region, where the heat generation rate and the heat loss through cell case are balanced with each other. After 2–3 min, as the stored electrical energy is nearly consumed, the heat generation becomes slower and the temperature decreases, eventually back to the room temperature. The temperature decrease rate is around 0.4°C/min, much lower than the initial temperature increase rate.

Similar phenomena are observed in the impact tests. Upon impact, the cell case is indented, pressing and eventually breaking the cathode and the membrane separator, and deforming the anode. The fracture toughness of the electrode film can be estimated as $K_{\mathrm{IC}}^{\mathrm{e}} = Y F^* \sqrt{\pi a}/b_e t_e$ (Anderson, 2004), where Y is a geometric factor, F^* is the critical load, a is the defect size, and b_{e} and t_{e} are the width and the thickness of electrode film, respectively. Although the electrode film is about five times thicker than the current collector, its strength is weaker by more than 90%. Thus, $K_{\mathrm{Ic}}^{e}/K_{\mathrm{Ic}}^{c} \approx 1/50$, where K_{Ic}^{c} is the toughness of charge collector. The membrane separator is anisotropic (Chen et al., 2014a, 2014b). Its fracture strains are more than 200% in the fibrous direction

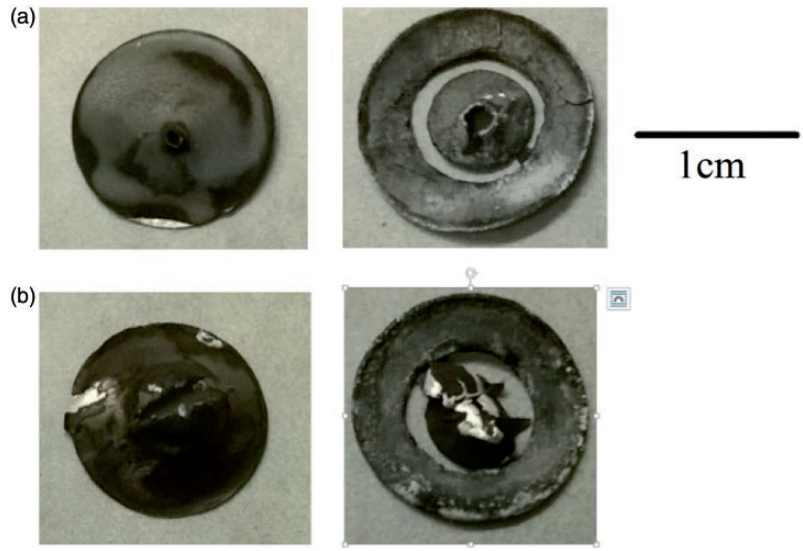

Figure 5. Typical reference electrode layers (left) and modified electrode layers (right) after (a) nail penetration and (b) impact tests.

and ~50% in the transvers direction, respectively. The failure is mainly associated with the growth and coalescence of the nanopores, influenced by the behaviors of ligaments. Assume that the membrane separator conforms to the indenter. The effective strain in the membrane separator during the dynamic indentation process would be $\varepsilon = [\arcsin\sqrt{1-(1-\tilde{x})^2}]/\sqrt{1-(1-\tilde{x})^2} - 1$, where $\tilde{x} = x/R_0$, x is the indentation depth, and $R_0 = 6.35\,\text{mm}$ is the radius of the indenter. When the indenter is compressed into the membrane separator by $\sim 0.9R_0$ or 5.7 mm, ε would exceed 50%. That is, although the membrane separator is strong and deformable along the fibrous direction, due to the highly heterogeneous impact loading mode and the anisotropic membrane properties, the cathode would be in direct contact with the anode. As the fully charged NMC532 grains are exposed to the Li disk, an internal shorting circuit is formed. With the low internal impedance, the heat generate rate, V^2/R, is higher than the heat loss rate, and therefore, the local temperature rises rapidly. In about 40 s, ΔT reaches the peak value. The initial temperature increase rate and the peak temperature are lower than those in the nail test, since the metallic nail is much more electrically conductive than NMC532, which leads to a lower internal impedance, R. Moreover, the post-peak temperature decrease is faster than that of the nail test, with the rate around 0.7°C/min.

In a modified battery cell, the cathode layer is patterned. The total NMC532 mass is nearly the same as in the reference cell, so is the stored electrical energy. In both nail penetration and impact tests, the breakage sites of the electrodes are near the center, as shown in Figure 5. Across the ring opening, the inner and outer parts of the electrode layer are not in direct contact. Consequently, as the penetrated or impacted sections of cathode and the anode are shorted, the effective resistance at the far field may increase. With the same electrode voltage, V, heat generation may be suppressed.

Figures 2 and 4 show the typical experimental data of modified battery coin cells. The temperature profiles of the modified cells are quite similar with that of reference cells, contradictory to the above expectations. The slight difference between them is within data scatter. In Figure 5, the outer sections of modified electrodes exhibit similar whitish markings as the inner sections, in both

nail and impact tests. The color change indicates the active participation of the NMC532 phase in exothermal reactions (Bandhauer et al., 2011), where local solid–electrolyte interface formation and electrolyte decomposition are accelerated. That is, in a modified cell, the ring opening does not block the electron transport, and the heat generation takes place throughout the entire electrode layer.

The specific energy of the Li-ion battery is quite high, around 200 W h/kg at the cell level (Thackeray et al., 2012); the energy tends to dissipate as internal shorting occurs. The similarity of the temperature profiles and the morphology of the reference and the modified cells suggest that the ring opening is insufficient to prevent heat generation and heat accumulation in the outer areas of electrodes, since the gap is bridged by electrically conductive cell components, such as the electrolyte and the electrode strips. In order to efficiently mitigate thermal runaway, more uniform increase in internal impedance must be achieved.

Concluding remarks

To summarize, heat generation characteristics of Li-ion battery coin half-cells with patterned electrodes were investigated. The cathode was discontinuous, containing a ring opening that separated the cathode layer into an inner part and an outer part. Both nail penetration and impact experiments were conducted. The experimental data indicated that the ring opening did not have a pronounced influence on the temperature profiles, which should be attributed to the conductive cell components bridging across the gap.

Declaration of Conflicting Interests

The author(s) declared no potential conflicts of interest with respect to the research, authorship, and/or publication of this article.

Funding

The author(s) disclosed receipt of the following financial support for the research, authorship, and/or publication of this article: This research was supported by the Advanced Research Projects Agency – Energy (ARPA-E) under Grant No. DE-AR0000396.

References

Anderson TL (2004) *Fracture Mechanics: Fundamentals and Applications*. Boca Raton, Florida: CRC Press.

Balakrishnan PG, Ramesh R and Prem Kumar T (2006) Safety mechanisms in lithium-ion batteries. *Journal of Power Sources* 155: 401–414.

Bandhauer TM, Garimella S and Fuller TF (2011) A critical review of thermal issues in lithium-ion batteries. *Journal of the Electrochemistry Society* 158: R1–R25.

Chen J, Sun T, Qi Y, et al. (2014a) A coupled penetration-tension method for evaluating the reliability of battery separators. *ECS Electrochemistry Letters* 3: A41–A44.

Chen J, Yan Y, Sun T, et al. (2014b) Deformation and fracture behaviors of microporous polymer separators for lithium ion batteries. *RSC Advances* 4: 14904–14914.

Etacheri V, Marom R, Elazari R, et al. (2011) Challenges in the development of advanced Li-ion batteries: A review. *Energy and Environmental Science* 4: 3243.

Feng XM, Ai XP and Yang HX (2004) A positive-temperature-coefficient electrode with thermal cut-off mechanism for use in rechargeable lithium batteries. *Electrochemistry Communications* 6: 1021–1024.

Harris SJ, Timmons A and Pitz WJ (2009) A combustion chemistry analysis of carbonate solvents used in Li-ion batteries. *Journal of Power Sources* 193: 855–858.

Iwamura S, Nishihara H, Ono Y, et al. (2015) Li-rich Li-Si alloy as a lithium-containing negative electrode material towards high energy lithium-ion batteries. *Scientific Reports* 5: Article no. 8085.

Le AV, Wang M, Shi Y, et al. (2015a) Heat generation of mechanically abused lithium-ion batteries modified by smooth fillers. *Journal of Physics D: Applied Physics* 48: 385501.

Le AV, Wang M, Shi Y, et al. (2015b) Effects of additional multiwall carbon nanotubes on impact behaviors of $LiNi_{0.5}Mn_{0.3}Co_{0.2}O_2$ battery electrodes. *Journal of Applied Physics* 118: 085312.

Liu C, Li F, Ma L-P, et al. (2010) Advance materials for energy storage. *Advanced Materials* 22: E38–E62.

Lu L, Han X, Li J, et al. (2007) A review on the key issues for lithium-ion battery management in electric vehicles. *Journal of Power Sources* 226: 272–288.

Thackeray MM, Wolvertonb C and Isaacsc ED (2012) Electrical energy storage for transportation—Approaching the limits of, and going beyond, lithium-ion batteries. *Energy and Environmental Science* 5: 7854.

Zhang SS (2007) A review on the separators of liquid electrolyte Li-ion batteries. *Journal of Power Sources* 164: 351–364.